Morphological clues to wet granular pile stability

M. SCHEEL[1], R. SEEMANN[1], M. BRINKMANN[1], M. DI MICHIEL[2], A. SHEPPARD[3], B. BREIDENBACH[4] AND S. HERMINGHAUS[1]*

[1]Max Planck Institute for Dynamics and Self-Organization, Bunsenstr. 10, D-37073 Göttingen, Germany
[2]European Synchrotron Radiation Facility, BP 220, F-38043 Grenoble Cedex, France
[3]Dept. Appl. Math., Australian National University, Canberra ACT 0200, Australia
[4]Institut für Theoretische Physik, Universität Erlangen-Nürnberg, Staudtstrasse 7, D-91058 Erlangen, Germany
*e-mail: stephan.herminghaus@ds.mpg.de

Published online: 10 February 2008; doi:10.1038/nmat2117

When a granular material such as sand is mixed with a certain amount of liquid, the surface tension of the latter bestows considerable stiffness to the material, which enables, for example, sand castles to be sculpted[1–4]. The geometry of the liquid interface within the granular pile is of extraordinary complexity and strongly varies with the liquid content[5–7]. Surprisingly, the mechanical properties of the pile are largely independent of the amount of liquid[2,8–13] over a wide range[14–16]. We resolve this puzzle with the help of X-ray microtomography, showing that the remarkable insensitivity of the mechanical properties to the liquid content is due to the particular organization of the liquid in the pile into open structures. For spherical grains, a simple geometric rule is established, which relates the macroscopic properties to the internal liquid morphologies. We present evidence that this concept is also valid for systems with non-spherical grains. Hence, our results provide new insight towards understanding the complex physics of a large variety of wet granular systems including land slides, as well as mixing and agglomeration problems.

It is a familiar experience at the beach that sand makes a mouldable material almost irrespective of the amount of water added: no-one needs a recipe to build a sand castle. Assemblies of wet glass spheres show the same basic phenomena as wet sand, and thus are widely used model systems[10–18]. Figure 1a shows data for three characteristic mechanical parameters of a wet pile of glass beads. The tensile strength, the yield stress and the critical acceleration at which fluidization sets in are plotted as a function of liquid content, W, in the range $0 < W \leq 0.15$. The latter is defined as the liquid volume divided by the total sample volume. Accordingly, $W = 0.15$ is equivalent to about 35% of the available pore space. Clearly, none of the three quantities depends significantly on the liquid saturation. Within the experimental uncertainties, all of the data points are consistent with the horizontal dashed line, which serves as a guide to the eye. The only exception is the sharp rise at very small W, where the transition from the dry state to the wetted state (capillary bridges) takes place[2,8–18]. This results from filling the crevices and roughness on the bead surfaces with liquid[16,19] and shall not concern us here any further. The fact that the mechanical properties are largely unaffected by the liquid content in the remaining, wide range of W corroborates the experience at the beach, and will be the subject of this article.

To obtain the details of the grain packing geometry and the liquid distribution within the pile, we carried out X-ray microtomography experiments with a variety of glass beads, including those used in our mechanical tests. The contact angle θ of the wetting liquid (Fig. 2d) was less than 10°, as determined independently by optical microscopy. The packing density of the wet pile was $\rho = 0.57 \pm 0.02$ throughout our experiments. In a series of experiments, we monitored the volumes of capillary bridges as a function of the time elapsed after sample preparation. Driven by differences in the Laplace pressure, the volumes of the individual bridges approached one another within a characteristic time of about 5 min, as illustrated in the inset of Fig. 3. Obviously, sufficient material transport takes place either through the gas phase or through the wetting layer on the beads[16,20]. Images for the analysis below were taken several hours after sample preparation to ensure full equilibration.

In Fig. 1b, the number of capillary bridges, the total number of liquid clusters (defined as connected regions of liquid wetting more than two beads) and the liquid volume of the biggest cluster are shown as functions of the liquid content. Clearly, substantial changes in the morphology of the liquid structures take place in the studied range. As W is increased, the liquid structures merge into larger clusters. At $W = 0.11$, the largest cluster contains about 90% of the liquid. Examples of the capillary bridges and smallest clusters that were found in our samples by X-ray tomography are shown in the top row of Fig. 2a. The bottom row shows the corresponding morphologies as obtained from numerical minimization of the interfacial free energy using the freely available software package Surface Evolver[21]. A fraction of a percolating cluster is shown in Fig. 2b.

In Fig. 2c, all emerging morphologies in a wet pile of spherical beads at $W = 0.035$ are represented by dots in the plane spanned by their liquid volume, V, and their total surface area, S (sum of the free liquid surface and the liquid–glass interface). At very small liquid volumes, we find a dense group of data points representing capillary bridges. At larger liquid volumes, other distinct groups corresponding to larger liquid clusters are visible. It is remarkable that all data points in Fig. 2c representing the various liquid structures group onto a single 'scaling curve'. For compact clusters, that is, liquid structures without air inclusions, it is straightforward to compute the expected surface-to-volume ratio for a pile of spherical beads. If R is the average radius of the glass spheres and N

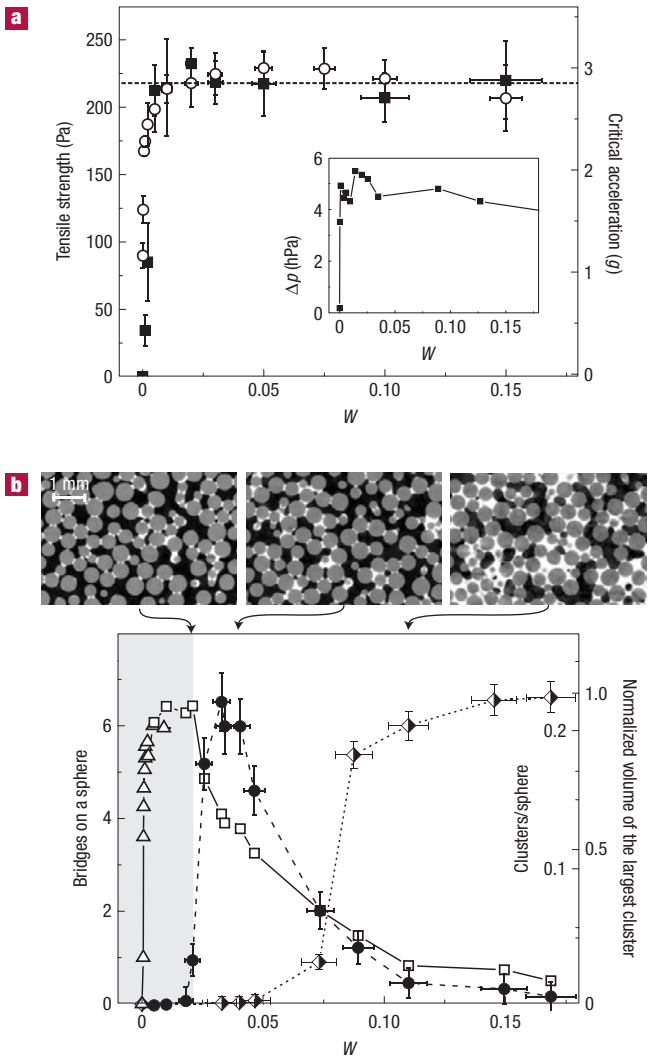

Figure 1 Stiffness of a wet granular pile in comparison with the reorganization of liquid structures. a, Mechanical properties: Tensile strength (filled squares), critical acceleration for fluidization (open circles). The dashed horizontal line is a guide to the eye. Inset: Yield stress[14]. **b**, Images: Sections through 3D tomograms of the analysed samples at $W = 0.02$, 0.04 and 0.11, from left to right. Main panel: Frequencies of liquid objects as extracted from X-ray tomography data. Left axis (open symbols): Average number of capillary bridges on a sphere (triangles: fluorescence microscopy[16]; squares: X-ray tomography). Right axis: Average number of clusters per sphere (filled symbols), and normalized volume of the largest cluster (half-filled symbols). In both **a** and **b**, the vertical error bars are standard deviations; the horizontal error bars reflect the experimental accuracy of determining the liquid volume.

is the number of beads in a box of volume V_0, the total surface area of these beads is $S = 4\pi NR^2$. As the volume fraction of the beads is $\rho = 4\pi NR^3/3V_0$, and the volume of the void space is given by $V = (1-\rho)V_0$, we readily find

$$S = \frac{3V\rho}{R(1-\rho)}. \qquad (1)$$

This is represented as the solid line in Fig. 2c, which is clearly remote from the experimental data. The dashed line indicates the surface-to-volume ratio of the largest liquid cluster we found at $W = 0.17$ (equivalent to about 40% filling of the available pore space). It provides a lower bound to the displayed data, and still lies by a factor of three above the solid line. This shows that the liquid forms ramified objects, in strong contrast to spontaneous imbibition from a liquid reservoir, which leads to compactly filled regions[22,23].

To put this result in perspective, we have to take a closer look at the geometrical details of the liquid structures within the granular pile. Consider a dense random pile of spheres, where the liquid makes a contact angle θ with the surface of the spheres. A capillary bridge between adjacent spheres with separation s is shown schematically in the inset of Fig. 2d. As can be seen from our tomographic data, s is very small for all capillary bridges and will be assumed equal to zero in the following consideration. In this case, the Laplace pressure in a capillary bridge, p_{cb}, is easily derived assuming a toroidal shape of the liquid surface[24,25]:

$$p_{cb}(\beta,\theta) = -\frac{\gamma}{R}\left[\frac{\cos(\beta+\theta)}{1-\cos\beta} - \frac{1}{\sin\beta}\right], \qquad (2)$$

where γ is the surface tension of the liquid and β is the bridge angle (Fig. 2d). Similarly, it is straightforward to obtain the volume of a capillary bridge, $V_{cb}(\beta,\theta)$, as a (lengthy) closed expression[24,25].

Next, we consider the transformations that are expected to take place when the amount of liquid is gradually increased. Initially, this demands an increase of the bridge angle β, and hence of the area of the glass surface that is covered by each capillary bridge. At the same time, the magnitude of the Laplace pressure, $|p_{cb}|$, becomes smaller according to equation (2). These effects cancel each other almost exactly as far as the mutual force on the spheres is concerned, because this is mainly given by p_{cb} multiplied by the projected area of liquid contact[6,24], $\pi(R\sin\beta)^2$. As a result, the mutual attraction of the glass spheres remains roughly constant at $2\pi R\gamma\cos\theta$.

At larger liquid content, however, neighbouring bridges will touch each other and coalesce forming larger agglomerates. As is evident from the inset of Fig. 2d, the minimum value of β at which coalescence may take place in a dense regular packing of equally sized spheres is $\beta^* = \pi/6 = 30°$. This value of the maximum bridge angle corresponds to an equilateral triangular configuration, that is, three spheres in mutual contact. The corresponding Laplace pressure $p^* = p_{cb}(\beta^*,\theta)$ is equal to $-(1+2\sqrt{3})\gamma/R \approx -4.46\gamma/R$ for complete wetting $\theta = 0°$. Whenever two capillary bridges located on the same sphere come into contact and coalesce, the 'triangular' opening between the sphere and two of its neighbours will be filled with liquid. Hence, this type of coalescence event invariably involves three adjacent spheres. The resulting morphology, which we call a trimer, is shown in Fig. 2a. Except for the central part, its shape is almost identical to the union of three capillary bridges before coalescence at the corresponding Laplace pressure of the trimer.

A statistical analysis of the tomography data reveals that the $\pi/6$ rule for the coalescence of capillary bridges is still applicable to our randomly packed pile of glass beads. The measured distribution of angular distances between contact points shown in Fig. 2d exhibits a sharp peak at 60°, reminiscent of the regular arrangement of equally sized spheres (the smaller peak at ≈115° may be attributed to ideal bipyramidal configurations). Angular distances below 60°, however, are virtually absent. Larger liquid structures will emerge in the pile by consecutive fusion of smaller clusters at their outer loops once the Laplace pressure comes close to the critical value, p^*. The coalescence also leads to a rather open liquid morphology for larger clusters, just as observed in the experiments (Fig. 2). The fused capillary bridges that constitute the cluster appear as loop structures in the X-ray tomograms.

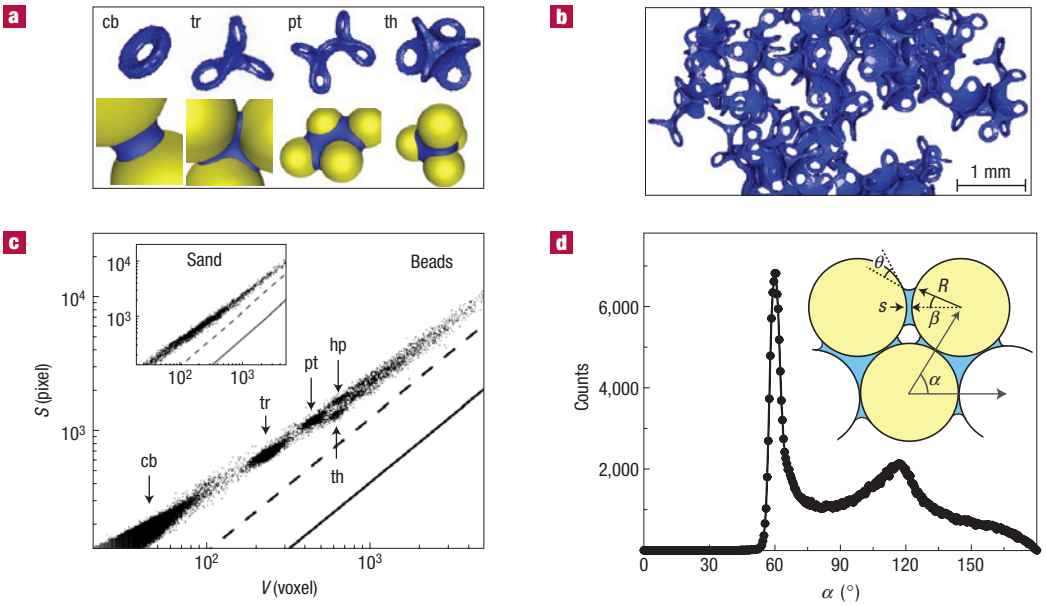

Figure 2 Liquid morphologies in a wet granular pile. a, Top row: Capillary bridge (cb), trimer (tr), pentamer (pt) and filled tetrahedra (th) as obtained from X-ray tomography. Bottom row: As obtained numerically. **b**, Fraction of a large percolating liquid cluster (X-ray tomography, see Supplementary Information). **c**, Cumulative plot of the total liquid surface area versus the volume of all clusters appearing at $W = 0.035$, as obtained by X-ray microtomography (hp: heptamers). Distinct groups of points, which correspond to the structures assigned to them, can be clearly identified. The solid line represents the solution to equation (1). The dashed line represents the surface-to-volume ratio of the largest cluster we found ($\sim 10^7$ voxel, at $W = 0.17$). Inset: Same plot for all clusters appearing at $W = 0.07$ within a wet sand pile. **d**, Distribution of angular distances between two neighbouring contact points (threshold separation 0.05 R). Inset: Schematic diagram of a capillary bridge at bead separation s, and two trimers.

The experimental data points in Fig. 3 demonstrate that the Laplace pressure in equilibrated samples levels off above a certain critical liquid content W^* in accordance with the critical value p^*. Here, we have used the size of capillary bridges at zero separation as a pressure probe. Using the volume of a critical bridge[23,24] at $s = 0$, $V_{cb}(\beta^*, \theta = 0) \approx 0.058R^3$ and the average number of capillary bridges per sphere, we can estimate the critical liquid content at which the bridges start to coalesce as $W^* \approx 0.024$. This agrees well with the observed transition at the right border of the grey shaded area in Fig. 1b, as well as the crossover to the plateau of the Laplace pressure shown in Fig. 3.

On the basis of a more general argument, it can be seen that the Laplace pressure is limited by the critical value p^* even on timescales well below the equilibration time between individual liquid clusters. Consider two disconnected loops, or capillary bridges, sharing a triangular configuration (yellow circles in the inset of Fig. 2d). At any triangular configuration, the angular distance α between the contact points represents a limit to the sum of the opening angles β for a pair of adjacent loops. Owing to the generic angular distance, $\alpha \approx 60°$, the probability that an overcritical loop, that is, with a Laplace pressure $p > p^*$, has another overcritical loop as its neighbour is very small. Hence, the probability for an overcritical cluster to survive in the pile will become exponentially small as the number of loops in the cluster grows. Any coalescence of two neighbouring clusters at a triangular configuration is accompanied by a drop in the Laplace pressure, but this drop becomes smaller in size as the clusters grow. From these observations, we may conclude that the Laplace pressure of a large cluster will be close to the critical value p^*. In contrast to the exchange of liquid between different clusters (Fig. 3, inset), equilibration within a single cluster is fast. This implies that the above arguments can also be applied to driven systems including, for instance, sheared granulates (Fig. 1a, inset).

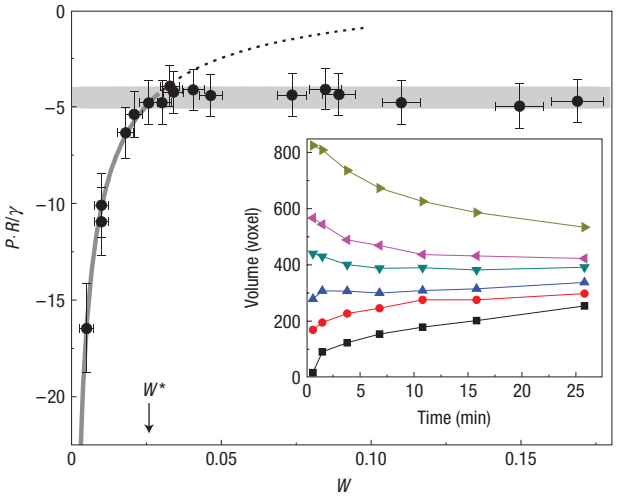

Figure 3 Normalized Laplace pressure within liquid structures in a wet pile of glass beads. The solid line denotes the theoretical expectation for individual capillary bridges. It is continued as dotted above W^*. The grey bar indicates the expected values of $p_{cb}(\beta^*, \theta)$ for $0 < \theta \leq 10°$, according to equation (2). The Laplace pressure has been normalized with the surface tension, γ, and average radius of the spheres, R. Inset: Volume of individual capillary bridges as a function of the time after fluidization. The characteristic timescale of the volume exchange is about 5 min. The vertical error bars are experimental uncertainties due to the finite resolution of the microtomography; the horizontal error bars reflect the experimental accuracy of determining the liquid volume.

As a consequence of the coalescence process, the liquid morphology of wet piles consists mainly of set unions of capillary

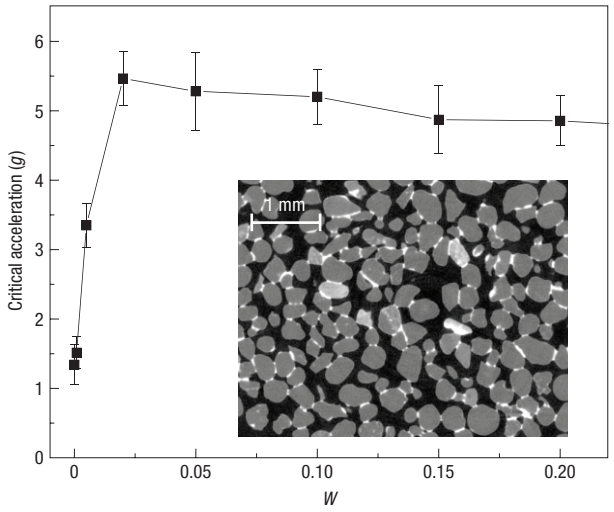

Figure 4 Stiffness of a wet granulate consisting of non-spherical grains. Critical acceleration for fluidization by vertical agitation, determined for sand wetted by water. The error bars are standard deviations. Inset: Section through a 3D tomogram of the sample at $W = 0.03$.

bridges (of which the trimers are among the smallest), such that the projected area over which the Laplace pressure acts, and hence the mechanical strength of the material, is virtually unchanged as the clusters grow. It should be noted that the number of liquid bonds, that is, pairs of adjacent beads being wet by the same liquid cluster or capillary bridge, increases slowly with W (by roughly 10% in the range between W^* and $W = 0.1$). This is due to the formation of new liquid bonds between neighbouring spheres at non-zero separation. However, because the capillary force drops off quickly as the separation between the beads increases[24], these extra liquid bonds will hardly contribute to the mechanical properties of the pile, in accordance with our observations.

So far, we have only considered spherical grains, which is an idealized system when compared with a 'real' granulate. However, although the geometry of a pile of non-spherical grains is expected to be different[26], a generic geometry of closest packed neighbours will doubtlessly exist. It is thus expected that a geometrical rule similar to the $\pi/6$ rule discussed above will hold as well, depending on the size distribution and shape of the grains. Therefore, the basic mechanism of fixing the Laplace pressure to a characteristic value independent of W (at least for larger clusters) should essentially be the same. To support this conclusion we have carried out mechanical experiments on irregularly shaped sand. Figure 4 shows the critical acceleration for fluidization by vertical agitation as a function of the liquid content for sand grains. We obtain the same qualitative picture as shown in Fig. 1a: there is no appreciable dependence over the wide range of liquid content investigated ($0 < W \leq 0.2$). The increase of the critical acceleration for small liquid contents is broadened compared with the results shown in Fig. 1a for glass spheres owing to the extra crevices on the grains that have to be filled before capillary bridges can form. Further important evidence is shown in the inset of Fig. 2c. We find that within experimental scattering, all of the emerging liquid morphologies in the wet sand pile (shown for $W = 0.07$) group on the same 'scaling curve' as the liquid morphologies found within the glass beads. This corroborates the universality of the concepts we have presented above and explains the remarkable insensitivity of the mechanical properties of wet granulates with respect to their liquid content.

METHODS

Most of the experiments were carried out with glass beads with an average diameter of 280 μm purchased from Whitehouse Scientific. The polydispersity of about 10% was sufficient to prevent crystallization. Sand grains were obtained by sieving regular sand (received from a glacial deposit near Marzahne, Brandenburg, Germany) to reduce the width of the size distributions to range from 355 to 500 μm. The samples for the mechanical tests and the X-ray tomography studies were prepared by thoroughly mixing a certain liquid volume with a certain volume of dry granulate. In all experiments, the contact angles of the wetting liquids were below 10°.

The X-ray microtomography experiments were carried out at the ESRF synchrotron in Grenoble. The measurements were carried out at the High Energy Scattering Beamline ID15A using 'white' X-ray radiation generated by a wiggler source with a peak photon energy of 40 keV. The imaging set-up consisted of a scintillator screen, which converts the X-rays into visible light, and a fast CCD (charge-coupled device) camera equipped with a ×1 macro-objective. The spatial resolution was 14 μm and the detector field of view 14 mm × 14 mm (ref. 27). As the wetting liquid, an aqueous zinc iodide solution was used with densities ranging from 1.3 to 2.6 g ml^{-1} depending on W to optimize contrast in the images. The measured interfacial tension (pending drop method) was equal to the value for water within our accuracy. The capillary length remained large compared with the diameter of the spheres throughout. The samples were given at least 24 h to equilibrate before the measurements.

Typically, a tomographic data set consisted of 900 projections acquired within about 20 s at equally spaced angular position, covering a total angle of 180°. The three-dimensional (3D) microstructure of the sample was reconstructed from the sets of 2D projections using a standard filtered back-projection algorithm.

MECHANICAL TESTS

To determine the critical acceleration for fluidization by vertical agitation, a fluidized sample (large agitation amplitude) was first quenched into a solid state by ramping down the agitation amplitude. The agitation was then slowly increased until fluidization set in[14,15]. The presented measurements were carried out at an agitation frequency of 200 Hz, whereby the critical fluidization amplitudes were much smaller than the diameter of the beads.

The tensile strength was determined by rotating a horizontal plastic tube filled with wet granulate, around a vertical axis. The angular velocity was slowly increased until the granular plug ruptured. The centrifugal forces at failure were determined from the size of the granular plug and the rotational speed at failure and corrected for the friction force of the granulate at the tube walls.

A custom-made shear cell was used to shear the granulate periodically between two rubber membranes with a parabolic shear profile at constant absolute pressure. The yield stress was determined from the differential pressure, Δp, between the two membranes[6,14].

Whenever a sample was sheared or agitated, the resulting packing density was found to be 0.57 ± 0.02, which is a robust value for this system. For comparison, samples with the same packing density were used in both X-ray tomography and all mechanical tests.

X-RAY TOMOGRAPHY

The reconstructed tomography images were filtered and segmented using the Mango 3D imaging toolkit[28]. The noise was reduced by a hybrid anisotropic diffusion edge-preserving smoothing filter[29]. Segmentation was then carried out using the method of converging active contours[30]. First, a thresholding in the intensity-gradient space of the image identifies those voxels that can be unambiguously classified as one particular phase. These seed regions are then expanded to fill all of the space using a fast marching algorithm[31]. All subsequent image analysis was done using Matlab, enabling us to determine the volume and surface of each individual cluster.

The finite resolution of the tomography limits the fidelity of the imaging process. For instance, the small contact angle of the liquid at the glass surface of a bead is not properly reproduced. Furthermore, openings of finite diameter around the contact points are 'observed'. However, from the known geometry (contact angle, radii of the beads), the bridge shape can be numerically computed and the total volume can be inferred on the basis of the known liquid content.

NUMERICAL EVALUATION

Capillary bridges, trimers, pentamers and filled tetrahedra are local minima of the interfacial energy in particular wetting geometries which are given by the position of adjacent glass beads. Assuming ideal local configurations and a fixed liquid volume, the equilibrium shape of the liquid–vapour interface was computed by numerical minimization of the interfacial energy. Investigations were carried out using the free software Surface Evolver[21], which uses a dynamic triangulation of the liquid–vapour interface. Nodes were constantly introduced and removed to keep the desired quality of the triangular mesh. The surface of the glass beads, which is wetted by liquid, was not triangulated as its area was obtained directly by line integrals over suitable vector fields along the contact line. Different equilibrium contact angles were achieved through variation of the surface energies. A conjugate gradient descent was applied to minimize the interfacial energy, allowing for local constraints and the subsidiary condition of a fixed volume.

Received 29 June 2007; accepted 9 January 2008; published 10 February 2008.

References

1. Hornbaker, D. J., Albert, R., Albert, I., Barabási, A.-L. & Schiffer, P. What keeps sandcastles standing? *Nature* **387**, 765 (1997).
2. Nowak, S., Samadani, A. & Kudrolli, A. Maximum angle of stability of a wet granular pile. *Nature Phys.* **1**, 50–52 (2005).
3. Schiffer, P. A. Bridge to sandpile stability. *Nature Phys.* **1**, 21–22 (2005).
4. Lu, N., Wu, B. & Tan, C. P. Tensile strength characteristics of unsaturated sands. *J. Geotech. Geoenviron. Eng.* **133**, 144–154 (2007).
5. Iveson, S. M., Litster, J. D., Hapgood, K. & Ennis, B. J. Nucleation, growth and breakage phenomena in agitated wet granulation processes: A review. *Powder Tech.* **117**, 3–39 (2001).
6. Herminghaus, S. Dynamics of wet granular matter. *Adv. Phys.* **54**, 221–261 (2005).
7. Mitarai, N. & Nori, F. Wet granular materials. *Adv. Phys.* **55**, 1–45 (2006).
8. Rumpf, H. *Agglomeration* (AIME, Interscience, New York, 1962).
9. Gröger, T., Tüzün, U. & Heyes, D. M. Modelling and measuring of cohesion in wet granular materials. *Powder Tech.* **133**, 203–215 (2003).
10. Richefeu, V., El Youssoufi, M. S. & Radjaï, F. Shear strength properties of wet granular materials. *Phys. Rev. E* **73**, 051304 (2006).
11. Soulié, F., El Youssoufi, M. S., Cherblanc, F. & Saix, C. Capillary cohesion and mechanical strength of polydisperse granular materials. *Eur. Phys. J. E* **21**, 349–357 (2006).
12. Bocquet, L., Charlaix, É. & Restagno, F. Physics of humid granular media. *C. R. Physique* **3**, 207–215 (2002).
13. Pierrat, P. & Caram, H. S. Tensile strength of wet granular materials. *Powder Tech.* **91**, 83–93 (1997).
14. Fournier, Z. *et al.* Mechanical properties of wet granular materials. *J. Phys. Condens. Matter* **17**, S477–S502 (2005).
15. Scheel, M., Geromichalos, D. & Herminghaus, S. Wet granular matter under vertical agitation. *J. Phys. Condens. Matter* **16**, S4213–S4218 (2004).
16. Kohonen, M. M., Geromichalos, D., Scheel, M., Schier, C. & Herminghaus, S. On capillary bridges in wet granular materials. *Physica A* **339**, 7–15 (2004).
17. Tegzes, P., Vicsek, T. & Schiffer, P. Avalanche dynamics in wet granular material. *Phys. Rev. Lett.* **89**, 094301 (2002).
18. Samadani, A. & Kudrolli, A. Angle of repose and segregation in cohesive granular matter. *Phys. Rev. Lett.* **64**, 051301 (2001).
19. Halsey, T. C. & Levine, A. J. Critical angle of wet sandpile. *Phys. Rev. Lett.* **80**, 3141–3144 (1998).
20. Seemann, R., Mönch, W. & Herminghaus, S. Liquid flow in wetting layers on rough substrates. *Europhys. Lett.* **55**, 698–704 (2001).
21. Brakke, K. The surface evolver and the stability of liquid surfaces. *Phil. Trans. R. Soc. A* **354**, 2143–2157 (1996).
22. Geromichalos, D. *et al.* in *Contact Angle, Wettability and Adhesion* Vol. 3 (ed. Mittal, K. L.) (Diversified Enterprises, Claremont, 2003).
23. Geromichalos, D., Mugele, F. & Herminghaus, S. Nonlocal dynamics of spontaneous imbibition fronts. *Phys. Rev. Lett.* **89**, 104503 (2002).
24. Willett, C. D., Adams, M. J., Johnson, S. A. & Seville, J. P. K. Capillary bridges between two spherical bodies. *Langmuir* **16**, 9396–9405 (2000).
25. Fisher, R. A. On the capillary forces in an ideal soil; correction of formulae given by W. B. Haines. *J. Agric. Sci.* **16**, 492–505 (1926).
26. Donev, A. *et al.* Improving the density of jammed disordered packings using ellipsoids. *Science* **303**, 990–993 (2004).
27. Di Michiel, M. *et al.* Fast microtomography using high energy synchrotron radiation. *Rev. Sci. Instr.* **76**, 043702 (2005).
28. Averdunk, H. & Sheppard, A. The Mango 3D image analysis toolkit. http://xct.anu.edu.au/mango (2007).
29. Frangakis, A. S. & Hegerl, R. Noise reduction in electron tomographic reconstructions using nonlinear anisotropic diffusion. *J. Struct. Biol.* **135**, 239–250 (2001).
30. Sheppard, A. P., Sok, R. M. & Averdunk, H. Techniques for image enhancement and segmentation of tomographic images of porous materials. *Physica A* **339**, 145–151 (2004).
31. Sethian, J. A. *Level Set Methods and Fast Marching Methods: Evolving Interfaces in Computational Geometry, Fluid Mechanics, Computer Vision and Materials Science* (Cambridge Univ. Press, Cambridge, 1999).

Acknowledgements

The authors thank K. Mecke and K. Jacobs for valuable discussions. Support from the European Synchrotron Radiation Facility is gratefully acknowledged. We appreciate financial support from the DFG under grant Me1361/9 and within the SFB 755. The authors are indebted to Z. Khan and F. v. Bussel for critical reading of the manuscript.
Correspondence and requests for materials should be addressed to S.H.
Supplementary Information accompanies this paper on www.nature.com/naturematerials.

Author contributions

Experiments were carried out by M.S., R.S., M.DM. and S.H.; theory is by M.B. and S.H.; data analysis was done by M.S., R.S. and M.B.; numerical algorithms and implementation are by A.S. and B.B.